Properties of pseudospin polarization on a graphene-based spin singlet superconducting junction*

Jia Shuan-Wen(贾拴稳)[a], Wang Jun-Tao(王军涛)[b], Yang Yan-Ling(杨艳岭)[a], and Bai Chun-Xu(白春旭)[a]†

[a] School of Physics, Anyang Normal University, Anyang 455000, China
[b] Department of Mathematics, Henan Institute of Science and Technology, Xinxiang 453000, China

(Received 24 October 2012; revised manuscript received 28 January 2013)

We investigate theoretically transport characteristics in a graphene-based pseudospinmagnet/superconductor junction, including the s-wave and the d-wave pairing symmetry potential in the superconducting region. It is found that the pseudospin polarization, in sharp contrast to spin polarization in the graphene-based ferromagnet/superconductor junction, holds no influence on the specular Andreev reflection for a negligible Fermi energy. Furthermore, the Fano factor is crucially affected by the zero bias state. Therefore, we suggest here that the findings could shed light on the realization of graphene-based pseudospintronics devices and provide a new way to detect the specular Andreev reflection and the zero bias state in the actual experiments.

Keywords: graphene, anisotropic pairing symmetry, pseudospin polarization

PACS: 74.45.+c, 74.78.Fk, 72.80.Vp **DOI:** 10.1088/1674-1056/22/8/087408

1. Introduction

The new star material, graphene has become a subject of intense theoretical and experimental study since the successful fabrication was realized by Novoselov *et al.*[1,2] In graphene, the lattice can be viewed as a triangular lattice with a basis of two distinguishable atoms A and B per unit cell. The sublattice degree of freedom (A and B sublattices) is referred to as a "pseudospin". In the reciprocal-lattice space, the conduction band and valence band touch each other at two independent points K and K' (Dirac points). Those two Dirac points K and K' can be regarded as the "valley" degree of freedom. However, due to the degeneracy and chiral symmetry, the effective Hamiltonian of an intrinsic infinite graphene can be described by the Hamiltonian: $H_0^{\gamma} = -\mathrm{i}\hbar v_{\mathrm{F}}[\gamma\sigma_x\partial_x + \sigma_y\partial_y]$, where the $\gamma = \pm$ signs correspond to K and K' valleys, σ_x and σ_y are the Pauli matrix of pseudospin, and the Fermi velocity $v_{\mathrm{F}} \approx c/300$ with c being the speed of light. Such a peculiar and unique band structure gives rise to a number of unusual electronic properties in graphene such as the unconventional quantum Hall effect,[3–6] Klein tunneling,[7–9] and specular Andreev reflection (SAR),[10–15] and so on.

From the application point of view, the manipulation of the pseudospin for a pseudospintronics device is one of the hot topics in the graphene-based electronic device community at present.[16–21] Note that the concept of pseudospintronics was first proposed in the bilayer graphene material.[16] In particular, Majidi and Zareyan[21] have extended the study into the monolayer graphene setup.[21] Generally, similar to the physical spin, the "up" and "down" pseudospin states correspond to quasiparticle density solely on the A and B sublattice sites, respectively. Theoretically, there are both routes toward intrinsic pseudospin polarization[16–18,20,21] and suggestions of laser fields-induced pseudospin polarization in graphene layers.[19] Through those ways, the pseudospin symmetry can be broken, which leads to the realization of pseudospin polarized states in a monolayer graphene. Thus the studies on the transport of pseudospinmagnetic states through graphene-based junction have been undertaken.[16,17,20,21] Very recently, the interplay of the pseudospin degree of freedom with the Andreev reflection has already been investigated in the graphene pseudospinmagnet/superconductor (PM/S) junction.[22] It was shown that the pseudospin has a determinative effect on Andreev reflection and the proximity effect in the geometry.

Up to now, no conclusion about the interplay of the pseudospin degree of freedom with the anisotropic pairing symmetry has been exploited. The key point is that in sharp contrast to the physical spin, the pseudospin polarized lifts the pseudospin degeneracy, but it does not break the time-reversal symmetry. This leads to a principle problem not being answered: what is the novel feature in combining the pseudospinmagnetic states with the superconductivity with the anisotropic pairing symmetry? To the end, in this study we present the detailed investigations of the conductance and Fano factor of a graphene-based PM/S junction with the s-wave and d-wave pairing symmetry.

*Project supported by the National Natural Science Foundation of China (Grant Nos. 11147201 and U1204110) and the Key Project of the Chinese Ministry of Education (Grant No. 211100).

†Corresponding author. E-mail: chunxu_bai@yahoo.cn

© 2013 Chinese Physical Society and IOP Publishing Ltd

2. Theory and model

In this analysis, we consider a PM/S junction in the x–y plane as shown in Fig. 1, in which the ballistic normal (non-superconducting state) electrode occupies the region $x < 0$ (region PM), while the region $x > 0$ (region S) is in the superconducting state. The pseudospin polarized in PM can be induced by electron–electron interaction or the gap engineering.[16–18,20,21] Superconductivity in a graphene layer can be realized by the proximity effect[23–25] and the electron–phonon interaction or the repulsive electron–electron interaction, etc.[26–30] For the S electrode, the expressions of $\Delta(x)$ are taken to be $\Delta(x) = \Delta\exp(\mathrm{i}\phi)\Theta(x)$ and $\Delta(x) = \Delta\cos(2\theta_{\mathrm{S}} - 2\alpha)\exp(\mathrm{i}\phi)\Theta(x)$ for the s-wave and d-wave symmetries, respectively, where α denotes the orientation of the gap in k-space with regard to the interface, ϕ is the phase of the superconducting order parameter, θ_{S} the transmission angle, and $\Theta(x)$ the Heaviside step function. The potential profile $V(x)$ is expressed as $V(x) = V_0\Theta(x)$.

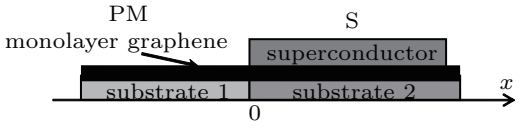


Fig. 1. Schematic diagram of a monolayer graphene PM/S junction. The substrates 1 and 2 are different and the former is used for creating an out-of-plane component of pseudospin in the left semi-infinite region. The superconducting stripe induces a non-zero superconducting pair potential in the right semi-infinite region by the proximity effect.

The Hamiltonian in the PM/S junction is time-reversal invariant and the Dirac–Bogoliubov–de Gennes (DBdG) equation can be written as[10,11]

$$\begin{pmatrix} H^{\gamma} - E_{\mathrm{F}} & \Delta(x) \\ \Delta^{*}(x) & E_{\mathrm{F}} - H^{\gamma} \end{pmatrix} \Psi_{\gamma} = E\Psi_{\gamma}, \tag{1}$$

with

$$H^{\gamma} = H_0^{\gamma} + h\sigma_z\Theta(-x) + V(x), \tag{2}$$

where h denotes the energy gap which is ensentialy important for acquiring the pseudospin polarized in PM.[21] $\Psi_{\gamma} = (u_{\gamma}, v_{\gamma})$ where $u_{\gamma} = (\psi_{\mathrm{A}\gamma},\ \psi_{\mathrm{B}\gamma})$ is the two-dimensional spinor for the electron–like quasiparticle and $v_{\gamma} = (\psi^{*}_{\mathrm{A}\bar{\gamma}},\ -\psi^{*}_{\mathrm{B}\bar{\gamma}})$ is the two-dimensional spinor for the hole-like quasiparticle. It is worthwhile to note that the interplay between magnetic order and unconventional superconducting pairing on the surface of a topological insulator has been investigated by a Hamiltonian similar to Eq. (1).[31–33] It is shown that the chiral Majorana mode (which exists at interface) is highly sensitive to the magnetization orientation. Despite of the similarity, in this study we mainly focus on the bulk conductance across a PM/S junction, while the detection and manipulation of the Majorana fermion bounded at the interface are the key points in those studies.[31–33]

Here we assume that an "up" electron with energy ε and transverse momentum q is incident on the interface from the left PM electrode, where the electron or hole wave propagates at an angle ϕ or ϕ' along x axis. So the wave functions in the two regions can be written as

$$\begin{aligned} \Psi_1 &= \Psi_{\mathrm{PF}}^{\mathrm{e}+} + r\Psi_{\mathrm{PF}}^{\mathrm{e}-} + r_{\mathrm{A}}\Psi_{\mathrm{PF}}^{\mathrm{h}-}, \\ \Psi_2 &= t\Psi_{\mathrm{S}}^{\mathrm{e}+} + t'\Psi_{\mathrm{S}}^{\mathrm{h}+}, \end{aligned} \tag{3}$$

where r and r_{A} are the amplitudes of normal and Andreev reflections in the left PF region, respectively, t and t' are the amplitudes of electron–like and hole-like quasiparticle in the S region.

By solving the DBdG equation (Eq. (1)), the wavefunctions in Eq. (3) can be expressed in a specific form. In the PM region, the wavefunctions are given by

$$\begin{aligned} \Psi_{\mathrm{PF}}^{\mathrm{e}\pm} &= (\pm\exp(\phi^{\mathrm{e}} \mp \mathrm{i}\phi),\ 1,\ 0,\ 0)\exp(\mathrm{i}(\pm k_{\mathrm{PF}}x + qy)), \\ \Psi_{\mathrm{PF}}^{\mathrm{h}\pm} &= (0,\ 0,\ \mp\exp(\phi^{\mathrm{h}} \pm \mathrm{i}\phi'),\ 1)\exp(\mathrm{i}(\mp k'_{\mathrm{PF}}x + qy)), \\ \sin(\phi) &= \hbar v_{\mathrm{F}}q/\sqrt{(\varepsilon + E_{\mathrm{F}})^2 - h^2}, \\ \sin(\phi') &= \hbar v_{\mathrm{F}}q/\sqrt{(\varepsilon - E_{\mathrm{F}})^2 - h^2}, \end{aligned} \tag{4}$$

where $\Psi_{\mathrm{PF}}^{\mathrm{e}\pm}$ and $\Psi_{\mathrm{PF}}^{\mathrm{h}\pm}$ are the wavefunctions traveling along the $\pm x$ directions for electron and hole, respectively, and $k_{\mathrm{PF}} = \sqrt{(\varepsilon + E_{\mathrm{F}})^2 - h^2} \times \cos(\phi)/\hbar v_{\mathrm{F}}$, and $k'_{\mathrm{PF}} = \sqrt{(\varepsilon - E_{\mathrm{F}})^2 - h^2} \times \cos(\phi')/\hbar v_{\mathrm{F}}$ are the momenta along the x axis. Note that the critical incident angle should be considered in the scattering process, and it is given by $\phi_{\mathrm{C}} = \arcsin(|k'_{\mathrm{PF}}|/k_{\mathrm{PF}})$. When the incident angle of the quasiparticle is larger than the critical angle, no Andreev process is permitted to take place.

In the S region, $\Psi_{\mathrm{S}}^{\mathrm{e}\pm}$ and $\Psi_{\mathrm{S}}^{\mathrm{h}\pm}$ in Eq. (3) represent the wave functions of the DBdG quasiparticles, which have the form shown below

$$\begin{aligned} \Psi_{\mathrm{S}}^{\mathrm{e}\pm} &= (u(\theta^{+}),\ \pm u(\theta^{+})\mathrm{e}^{\pm\mathrm{i}\theta^{+}},\ v(\theta^{+})\mathrm{e}^{-\mathrm{i}\varphi^{+}}, \\ &\quad \pm v(\theta^{+})\mathrm{e}^{\mathrm{i}(\pm\theta^{+} - \varphi^{+})})\mathrm{e}^{\mathrm{i}(\pm k_{\mathrm{S}}^{\mathrm{e}}x + qy)}, \\ \Psi_{\mathrm{S}}^{\mathrm{h}\pm} &= (v(\theta^{-}),\ \pm v(\theta^{-})\mathrm{e}^{\pm\mathrm{i}\theta^{-}},\ u(\theta^{-})\mathrm{e}^{-\mathrm{i}\varphi^{-}}, \\ &\quad \pm u(\theta^{-})\mathrm{e}^{\mathrm{i}(\pm\theta^{-} - \varphi^{-})})\mathrm{e}^{\mathrm{i}(\pm k_{\mathrm{S}}^{\mathrm{h}}x + qy)}, \end{aligned} \tag{5}$$

where

$$k_{\mathrm{S}}^{\mathrm{e(h)}} = (V_0 + E_{\mathrm{F}} + (-)\sqrt{\varepsilon^2 - \left|\Delta(\theta^{+(-)})\right|^2})\cos(\theta^{+(-)})/\hbar v_{\mathrm{F}},$$

the coherence factors are given by

$$u(\theta) = \sqrt{(1 + \sqrt{1 - |\Delta(\theta)/\varepsilon|^2})/2},$$

$$v(\theta) = \sqrt{(1 - \sqrt{1 - |\Delta(\theta)/\varepsilon|^2})/2},$$

$$\theta^{+(-)} = \theta_{\mathrm{S}}^{\mathrm{e}}(\pi - \theta_{\mathrm{S}}^{\mathrm{h}}),$$

and

$$\exp(\mathrm{i}\varphi^{\pm}) = \Delta(\theta^{\pm})/\left|\Delta(\theta^{\pm})\right|.$$

The transmission angle $\theta_S^{e(h)}$ for the electron-like (hole-like) quasiparticle is defined as follows: $\sin(\theta^{e(h)})/\sin(\phi) = \sqrt{(\varepsilon+E_F)^2-h^2}/(V_0+E_F+(-)\sqrt{\varepsilon^2-|\Delta(\theta^{e(h)})|^2})$. Note that for s-wave symmetry, $\Delta(\theta^{e(h)}) = \Delta$ since the electron–like and hole-like quasiparticles undergo a constant superconducting pairing potential.

The reflection amplitudes can be calculated by using the appropriate boundary conditions. Then it is straightforward to determine the tunneling conductance and shot noise. Unlike the tunneling conductance, from which the average transmission feature can be deduced, measurements of the shot noise can provide useful information relevant to the actual distribution of the transmission eigenvalues. Here we will calculate the tunneling conductance and Fano factor. The zero temperature tunneling conductance is defined as

$$G(eV) = G_0 \int_0^{\phi_C} (1-R+R_A)\cos(\phi)\,d\phi, \tag{6}$$

where $R = |r|^2$, $R_A = |r_A|\cos(\phi')/\cos(\phi)$, and $G_0 = 4e^2N(eV)/h$ is the ballistic conductance of metallic graphene, V is the bias voltage, and $N(eV) = (E_F+eV)w/(\pi\hbar v_F)$ denotes the number of available channels for a graphene sample of width w.

Similarly, we can also study the zero temperature Fano factor in the system, which is expressed as[34]

$$F = \int_0^{\phi_C} (R(1-R)+R_A(1-R_A)+2RR_A) \times \cos(\phi)\,d\phi \Big/ \int_0^{\phi_C} (1-R+R_A)\cos(\phi)\,d\phi. \tag{7}$$

Based on Eqs. (6) and (7), the tunneling conductance and Fano factor for the present PM/S junction can be obtained easily.

3. Numerical results and discussion

We start with the analysis of the results of s-wave superconducting pairing symmetry in Figs. 2(a) and 2(b). In the case of $h = 0$ (i.e., in the absence of the pseudospin polarization), we clearly recover the results of an N/S junction which has been studied in Refs. [10] and [11]. While for a nonzero h, several interesting features can be found. For $E_F = 100\Delta$, with the increase of h, the tunneling conductance decreases. The decrease feature of the tunneling conductance shows a great reduction of the value at $V = 0$, whereas the value at the gap edge ($eV = \Delta$) decreases much slower unless the pseudospin in pseudoferromagnet is almost polarized. When $h = E_F$, the tunneling conductance equals zero through all the energy region. However, for the case of $E_F = \Delta/100$, the situation becomes much different. On the whole, it shows that as h rises from 0 to E_F, the tunneling conductance keeps a constant value as a function of V. The result of the negligible bias voltage is extracted and plotted in the inset of Fig. 2(b). In the region, the characteristics can be found to be similar to those as shown in Fig. 2(a), owing to the domination of the retro-Andreev reflection (RAR) at small bias voltage for a nonzero Fermi energy $E_F = \Delta/100$. Those results reflect the fact that RAR is sensitive to the pseudospin polarization, whereas the SAR is just on the contrary. These observations may be understood by the following argument. Physically, the energy spectrum of graphene is the result of intersection of the energy bands stemming from sublattices A and B (see Fig. 3) and the chirality recommendation is allowed accordingly. Here the chiralities indicate the projections of pseudospin on the wave vector

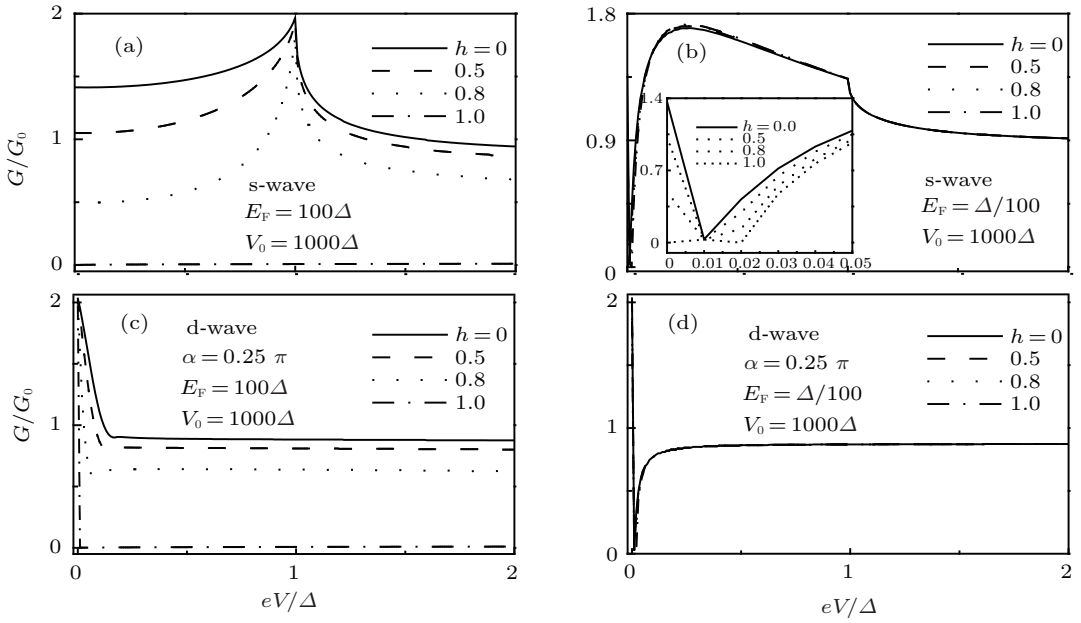


Fig. 2. Tunneling conductances through the PM/S junction as a function of incident energy eV for $E_F = 100\Delta$ (panels (a) and (c)) and $E_F = \Delta/100$ (panels (b) and (d)). Panels (a) and (b) and panels (c) and (d) correspond to s-wave and d-wave pairing symmetries with $\alpha = 0.25\pi$, respectively. Solid line, dashed line, dotted line, and dash–dotted line represent the results of $h = 0$, $0.5E_F$, $0.8E_F$, and E_F, respectively. The inset shows the very low bias voltage case for s-wave. In all panels, we set $V_0 = 1000\Delta$.

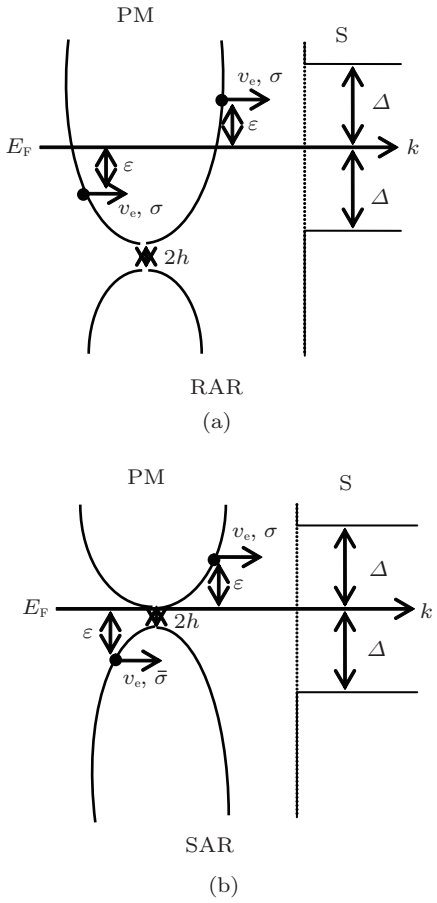


Fig. 3. Schematic diagrams of the spectrum of quasiparticles in single-layer graphene for RAR (a) and SAR (b).

(or momentum) which are positive and negative for electrons in conduction band and valence band, respectively.[7,10,11] On the other hand, as is well known, Andreev reflection is an important physical phenomenon peculiar to inhomogeneous superconductors. Actually, the Andreev reflection can be described using the pure electron language, as the two electrons (with opposite physical spin) enter into S and eventually join the condensate.[35–40] In graphene, the Andreev reflection may take place in the conduction band or the valence band.[10,11] For the conduction band, as shown in Fig. 3(a), an incident electron with σ (σ denotes the sublattice A) must combine an electron with σ due to the positive chirality and jumps into S with the same velocity vector. Meanwhile a conduction band Andreev reflection hole is left and stays in the sublattice A.[22] That is to say, the incident electron and conduction-band Andreev reflection hole propagate in the same sublattice. However, the divergence of the density of states between the incident electron and the conduction-band Andreev reflection hole increases with h increasing. Thus the effect of pseudospin polarization is to impose an encumbrance on the RAR and hence the Andreev conductance. While in the valence band, as shown in Fig. 3(b), an incident electron with σ must combine a valence-band electron with $\bar{\sigma}$ due to negative chirality and transfers into S.[7,10,11] In other words, the incident electron and valence-band Andreev reflection hole origin from the opposite sublattice.[22] But, for the case of $E_F = \Delta/100$, the densities of states of the incident electron and the valence-band Andreev reflection hole almost keep constant with the increase of h. So the effect of pseudospin polarization is of no use. Those are why we can find the distinct features for the two kinds of Andreev reflections in Figs. 2(a) and 2(b).

We now consider the difference between the s-wave and the d-wave superconducting pairing symmetries ($\alpha = 0.25\pi$). The main effect of the anisotropic symmetry is the appearance of the zero energy bound state and exhibits a peak at low bias. Indeed, it is clear from the figures that a zero bias conductance peak is formed and the conductance sharply drops off with bias increasing. Furthermore, a significant result of d-wave symmetry is that the zero bias conductance peak cannot be destroyed by the pseudospin polarization even in the full polarization condition for the cases of $E_F = 100\Delta$ and $E_F = \Delta/100$. On the other hand, in ferromagnet/superconductor (F/S) junction, the dependence of zero bias conductance on spin polarization is qualitatively different. It is shown that zero bias conductance decreases monotonically with the spin polarization of the ferromagnet.[41,42] It reflects the damaging of the zero energy bound state as the spin polarization increases. The contrary behavior can be ascribed to the difference in mechanism between the pseudospin polarization and the spin polarization. Physically, the pseudospin polarization induces an energy splitting that lifts the pseudospin degeneracy, but the energy splitting does not break the time-reversal symmetry, unlike the spin polarization in ferromagnet.

Next, we also study the dependences of the conductance on h/E_F in Figs. 4(a) and 4(b) for two different bias voltages: $eV = 0$ and Δ. The parameters are the same as those in Fig. 2 and the results are only for the s-wave symmetry case. For $eV = 0$, the conductances in both the $E_F = 100\Delta$ and $E_F = \Delta/100$ cases decrease monotonically with h/E_F increasing and vanish at $h = E_F$. This stems from the fact that the RAR dominates for the case of $E_F = \Delta/100$ at $eV = 0$. Therefore they behave in the same manner. Importantly, we see that at $eV = \Delta$ the situation becomes much intriguing, where the conductance of $E_F = \Delta/100$ is independent of h/E_F even at $h/E_F = 1$. In this regime the RAR will dominate for the case of $E_F = 100\Delta$, while the SAR will dominate for the case of $E_F = \Delta/100$. Moreover, in contrast to the graphene-based F/S junction case where the zero bias conductance attenuates linearly with the spin polarization increasing,[42] which exhibits a richer structure in the present junction. Thus, the intriguing and important feature revealed in Fig. 4 is that while the pseudospin polarization diminishes the RAR amplitude and hence the conductance, the SAR process completely overlooks

the pseudospin polarization. These phenomena are consistent with those in Fig. 2 and can be understood by the same way as that stated above. It is worthwhile to note that for the case of RAR, the conductances of pseudomagnet and ferromagnet junction show the similar characters to a function of polarization, but they origin from the different physical mechanisms. Nevertheless, for the case of SAR, the conductances of the two types of junctions display perfectly distinct behaviors, owing to the difference between the dependence on SAR and that on polarization.

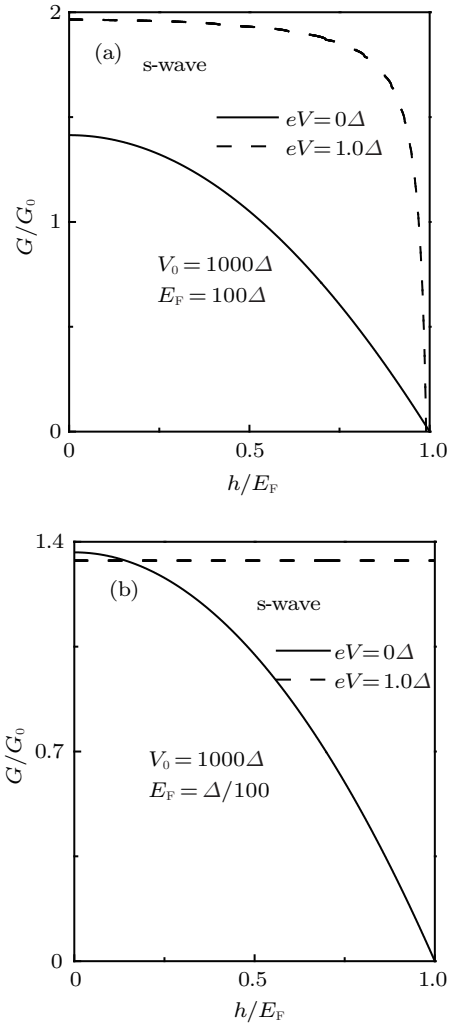


Fig. 4. Conductances versus h/E_F for the case of $E_F = 100\Delta$ (a) and $E_F = \Delta/100$ (b). The parameters are shown in the figure.

Finally, we come to look at some more certifications which provide additional qualitative support for the above picture. Here we calculate the Fano factor and show that its value crucially depends on whether the zero bias state exits. Figures 5(a) and 5(b) both show the zero bias Fano factors as a function of h/E_F for different orientations of the superconducting gap in S. For $\alpha \neq 0.25\pi$, as shown in Fig. 5, the Fano factors increase from the initial value ($h = 0$) to twice the Poisson noise for the perfect polarization case ($h/E_F = 1$). This is consistent with the result of conventional F/S junction, although the initial increase is very slow in conventional F/S junction.[43] However, it is drastically different from the scenario for the graphene-based F/S junction.[42,44] Physically, the difference in mechanism between spin and pseudospin polarization, leads to the fact that the zero bias Fano factor is saturate at two distinct values. However, for $\alpha = 0.25\pi$, the zero bias Fano factor is independent of the pseudospin polarization and equal to zero. The result suggests that a zero bias state results in a zero Fano factor and also it arises only near $\alpha = 0.25\pi$.[14,15] It is different from what is observed in conventional N/S junction, where the Fano factor is enhanced as compared with s-wave superconductor in the ballistic limit.[45] Those features about the zero bias Fano factor should be easily observable in experiment, and provide a direct way of testing the special characteristics of the PM/S junction.

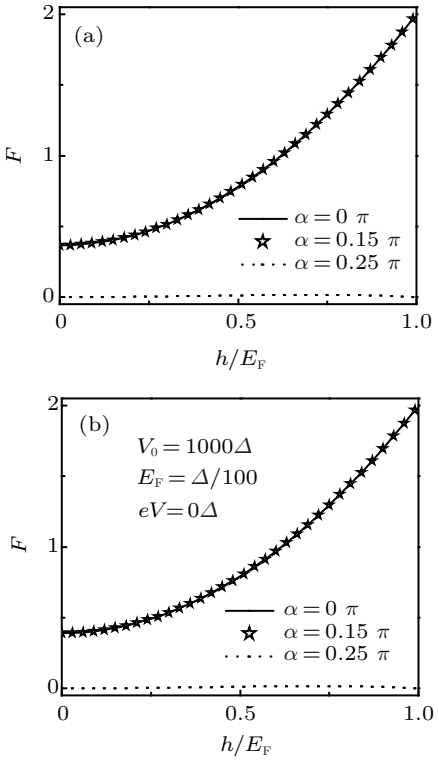


Fig. 5. Fano factors versus h/E_F for the cases of $E_F = 100\Delta$ (a) and $E_F = \Delta/100$ (b). The solid lines, star lines, and dotted lines correspond to $\alpha = 0$, 0.15π, and 0.25π, respectively. The other parameters are shown in the figure.

4. Conclusions

In this paper, we show that pseudospin polarization suppresses the RAR instead of the unrelated behavior which is typically found in the SAR case (for negligible Fermi energy). Meanwhile, it is also sensitive to the orientation of the gap α. Furthermore, the Fano factor is drastically different from those in the conventional N/S junction and graphene-based F/S junction. We can expect that our findings could give a ref-

erence for realizing graphene-based pseudospintronics device and provide a heuristic pathway for distinguishing the SAR and the zero bias state in the actual experiments in the near future.

References

[1] Novoselov K S, Geim A K, Morozov S V, Jiang D, Zhang Y, Dubonos S V, Grigorieva I V and Firsov A A 2004 *Science* **306** 666
[2] Tian H and Wang J 2012 *Chin. Phys. B* **21** 017203
[3] Novoselov K S, Geim A K, Morozov S V, Jiang D, Katsnelson M L, Grigorieva I V, Dubonos S V and Firsov A A 2005 *Nature* **438** 197
[4] Zhang Y, Tan Y W, Stormer H L and Kim P 2005 *Nature* **438** 201
[5] Gusynin V P and Sharapov S G 2005 *Phys. Rev. Lett.* **95** 146801
[6] McCann E and Falko V 2006 *Phys. Rev. Lett.* **96** 086805
[7] Katsnelson M L, Novoselov K S and Geim A K 2006 *Nat. Phys.* **2** 620
[8] Bai C and Zhang X 2007 *Phys. Rev. B* **76** 075430
[9] Pereira J M, Vasilopoulos J P and Peeters F M 2007 *Appl. Phys. Lett.* **90** 132122
[10] Beenakker C W J 2006 *Phys. Rev. Lett.* **97** 067007
[11] Beenakker C W J 2008 *Rev. Mod. Phys.* **80** 1337
[12] Bhattacharjee S and Sengupta K 2006 *Phys. Rev. Lett.* **97** 217001
[13] Bhattacharjee S, Maiti M and Sengupta K 2007 *Phys. Rev. B* **76** 184514
[14] Linder J and Sudbo A 2007 *Phys. Rev. Lett.* **99** 147001
[15] Linder J and Sudbo A 2008 *Phys. Rev. B* **77** 064507
[16] San-Jose P, Prada E, McCann E and Schomerus H 2009 *Phys. Rev. Lett.* **102** 247204
[17] Xia F, Farmer D B, Lin Y and Avouris P 2010 *Nano Lett.* **10** 715
[18] Min H, Borghi G, Polini M and MacDonald A H 2008 *Phys. Rev. B* **77** 041407(R)
[19] Zhou J 2008 arXiv: 0807.0667v1[cond-mat].
[20] Trushin M and Schliemann J 2011 *Phys. Rev. Lett.* **107** 156801
[21] Majidi L and Zareyan M 2011 *Phys. Rev. B* **83** 115422
[22] Majidi L and Zareyan M 2012 *Phys. Rev. B* **86** 075443
[23] Heersche H B, Jarillo-Herrero P, Oostinga J B, Vandersypen L M K and Morpurgo A F 2007 *Nature* **446** 56
[24] Miao F, Wijeratne S, Zhang Y, Coskun U C, Bao W and Lau C N 2007 *Science* **317** 1530
[25] Du X, Skachko I and Andrei E Y 2008 *Phys. Rev. B* **77** 184507
[26] Uchoa B and Castro Neto A H 2007 *Phys. Rev. Lett.* **98** 146801
[27] Kopnin N B and Sonin E B 2008 *Phys. Rev. Lett.* **100** 246808
[28] Profeta G, Calandra M and Mauri F 2012 *Nat. Phys.* **8** 131
[29] McChesney J L, Bostwick A, Ohta T, Seyller T, Horn K, González J and Rotenberg E 2010 *Phys. Rev. Lett.* **104** 136803
[30] Einenkel M and Efetov K B 2011 *Phys. Rev. B* **84** 214508
[31] Tanaka Y, Yokoyama T and Nagaosa N 2009 *Phys. Rev. Lett.* **103** 107002
[32] Linder J, Tanaka Y, Yokoyama T, Sudbo A and Nagaosa N 2010 *Phys. Rev. Lett.* **104** 067001
[33] Linder J, Tanaka Y, Yokoyama T, Sudbo A and Nagaosa N 2010 *Phys. Rev. B* **81** 184525
[34] Anantram M P and Datta S 1996 *Phys. Rev. B* **53** 16390
[35] Yang Y, Yang Z and Wang J 2012 *Chin. Phys. B* **21** 057402
[36] Liang J, Nie Y and Ye C 2011 *Chin. Phys. B* **20** 127202
[37] Jin B, Peng J and Yu H 2010 *Chin. Phys. B* **19** 087203
[38] Dou X and Xu M 2010 *Chin. Phys. B* **19** 067301
[39] Wang Z, Peng J and Yu H 2009 *Chin. Phys. B* **18** 5485
[40] Wang Z, Yu H and Peng J 2008 *Chin. Phys. B* **17** 4627
[41] Zutic I and Valls O T 2000 *Phys. Rev. B* **61** 1555
[42] Zhou J and Jin G 2009 *Europhys. Lett.* **87** 27008
[43] Jong M J M and Beenakker C W J 1995 *Phys. Rev. Lett.* **74** 1657
[44] Zhang Q, Fu D, Wang B, Zhang R and Xing D Y 2008 *Phys. Rev. Lett.* **101** 047005
[45] Zhu J X and Ting C S 1999 *Phys. Rev. B* **59** 14165